Structure and Mechanical Properties of Cr(Al)N/Al_2O_3 Nanocomposite Hard Coatings Fabricated by Differential Pumping Cosputtering

Masahiro Kawasaki*, Masateru Nose**, Ichiro Onishi***,
Kenji Matsuda****, and Makoto Shiojiri*****

*JEOL USA Inc., 11 Dearborn Road, Peabody,
Massachusetts 01960, USA, kawasaki@jeol.com
**Faculty of Art and Design, University of Toyama, Takaoka 933-8588, Japan
***JEOL Ltd., 3-1-2 Musashino, Akishima, Tokyo 196-8558, Japan
****School of Science and Engineering, University of Toyama, Toyama 930-8555, Japan
*****Kyoto Institute of Technology, Kyoto 606-8585, Japan, shiojiri@pc4.so-net.ne.jp

ABSTRACT

Cr(Al)N/Al_2O_3 hard coatings were fabricated by differential pumping cosputtering. Analytical electron microscopy revealed that the films sputter-deposited alternately by the CrAl and Al_2O_3 targets in the flow of Ar/N_2 and Ar, repsectively, grew in a columnar structure normal to the substrate. In a Cr(Al)N/17 vol.% Al_2O_3 film prepared at a substrate rotational speed of ω =12 rpm, each column comprised NaCl-type Cr(Al)N crystallites including homogeneously dispersive fine amorphous alumina particles (a-Al_2O_3). The indentation hardness (H_{IT}) and Young's modulus (E^*) increased with increasing ω. With increasing Al_2O_3 fraction, they increased once and then decreased. The maxima H_{IT} and E^* were obtained at 17 vol.% Al_2O_3, and they were H_{IT} = ~43 GPa and E^* = ~350 Gpa for the coating prepared at ω = 12 rpm. The a-Al_2O_3 particles worked as obstacles against the deformation of the Cr(Al)N lattices.

Key words: hard coating, Cr(Al)N/Al_2O_3, hardness, differential pumping cosputtering, analytical electron microscopy

1 INTRODUCTION

Nitrides of transition metals such as Ti, Zr and Cr are known as materials for hard or super hard coatings [1,2]. Much attention has been paid to studies of nanocomposite films of metal nitrides such as TiN/Si_3N_4, TiN/BN [3], and CrN/AlN [4], for improving hardness and saving rare metals. There are a few investigations on oxygen containing nanocomposite coating films. Stüber *et al*. reported an investigation of CrAlON films [5] and Kong *et al.* studied structure, mechanical properties and high-temperature oxidation resistance of AlN/SiO_2 coatings [6]. It is however still difficult to obtain nanocomposite films consisting of nitride and oxide by conventional reactive sputtering methods because of the high reactivity of oxygen to aluminum or titanium.

Nose *et al.* developed a differential pumping co-sputtering (DPCS) system, which has two chambers (P and Q) to sputter different materials and a rotating substrate holder [7]. The division of gas atmospheres in the DPCS system reduces cross-contamination, thus allowing to codeposite nitride and oxide by rapid rotation of the substrate.

Recently, we have investigated the structure and growth of a Cr(Al)N/SiO_x nanocomposite hard coating prepared on a Si substrate in the DPCS system [8,9]. The Cr(Al)N/SiO_x layer was deposited by cosputtering from two targets of CrAl and SiO_2 on the transition buffer layers of Cr(Al) and CrN, which were deposited under the different gas flow conditions from the CrAl target on the (001) Si substrate. Since the deposited oxide is not stoichiometric composition, we used the term SiO_x for the deposited silicon oxide. The prepared nanocomposite was Cr(Al)N/38 vol.% SiO_x, grown at a substrate rotational speed as low as ω = 1 rpm. This rotation speed was not optimal for the preparation of hard coating but we used it because our aim was to get the fundamentals of the deposition process in the DPCS [8]. In this paper, we report the mechanical property and the structure of the Cr(Al)N/Al_2O_3 layer prepared at various conditions in the DPCS system, to demonstrate its usefulness for fabricating super hard coatings.

2 EXPERIMENTALS

$Cr_{50}Al_{50}$ and Al_2O_3 targets were set in chambers P and Q in the DPCS system, respectively, and (001) Si wafers were set in the substrate holder heated at 250°C. The substrate holder was rotated at a speed of ω = 12 rpm. First, three depositions I, II, and III were successively performed on the Si substrates by sputtering only from the CrAl target in chamber P. The sputtering-deposition conditions are illustrated in Table 1. The RF power for the magnetron sputtering depositions was 200 W. The deposited films were the transition buffer layers to promote adhesion between the composite film and substrate. Except for the substrate rotational speed of ω = 12 rpm, the preparation conditions of the gas flow and the RF power for these transition layers were the same as those used for the previous Cr(Al)N/SiO_x nanocomposite coatings [8,9]. Next, the main deposition IV

Deposition	Chamber P Target $Cr_{50}Al_{50}$			Chamber Q Target Al_2O_3		Substrate rotational speed: ω =12 rpm	
	Ar (sccm)	N_2 (sccm)	Power (W)	Ar (sccm)	Power (W)	Time (minute)	Deposited film
I	10	0	200			8.17	B: *a*-SiO_x, *a*-Al_2O_3, Cr(Al) C: Cr(Al), *a*-Al_2O_3
II	10	10	200			29.37	D: CrN, Cr(Al), *a*-Al_2O_3
III	10	20	200			36.18	E: CrN, *a*-Al_2O_3
IV	10	20	200*	20	100*	810.0	F: Cr(Al)N, *a*-Al_2O_3

Table 1: Sputtering-deposition conditions for the transition buffer layers I, II, and III and main composite layer IV, and the structure of the deposited films. * RF powers which were used to prepare Cr(Al)N/17 vol.%Al_2O_3.

was carried out by operating both the CrAl chamber P and the Al_2O_3 chamber Q, on the transition buffer layers rotated at the same speed. Different RF powers in the P and Q chambers were applied for preparing composite layers with different compositions: *e.g.* 200 W and 100 W (asterisked in Table 1) so as to obtain a nominal composition of Cr(Al)N/17 vol.%Al_2O_3.

The indentation hardness (H_{IT}) and Young's modulus (E^*) of the Cr(Al)N/Al_2O_3 nanocomposite coatings were measured using a nanoindentation system (Fischerscope, H100C-XYp) at room temperature. To obtain the surface hardness of the specimen without effects of the under layers and substrate, the load for the indentation with a triangular Berkovitch diamond pyramid was limited to keep the impression depth lower than 10% of the total film thickness. The samples were thinned with focused ion beam (FIB) for transmission electron microscopy (TEM) and scanning transmission electron microscopy (STEM). TEM and STEM analyses were performed with JEOL JEM-2800 and ARM200F microscopes at 200kV, similar to our previous experiments [8,9].

3 RESULTS AND DISCUSSION

Figure 1 shows a bright-filed (BF) STEM image and the corresponding high-angle annual dark-field (HAADF) STEM image of a cross section, normal to the substrate surface, of a Cr(Al)N/17vol. %Al_2O_3 coating with the transition layers deposited on the Si substrate rotated at ω = 12 rpm. Layers indicated as A~F can be distinguished in the images, in particular the HAADF-STEM image in Figure 1(b), which is mainly formed by thermal diffuse scattering of electrons or incoherent imaging of elastically scattered electrons and provides the atomic number (Z) contrast approximately proportional to the square of Z [10,11]. We made high-resolution (HR) TEM observation and electron diffraction (ED) analysis of these layers. Figure 2 shows energy dispersive X-ray spectroscopy (EDS) mappings and intensity line profiles. The following results were obtained from these experiments and are briefly shown in Table 1.

Layers B and C formed on the Si substrate A by

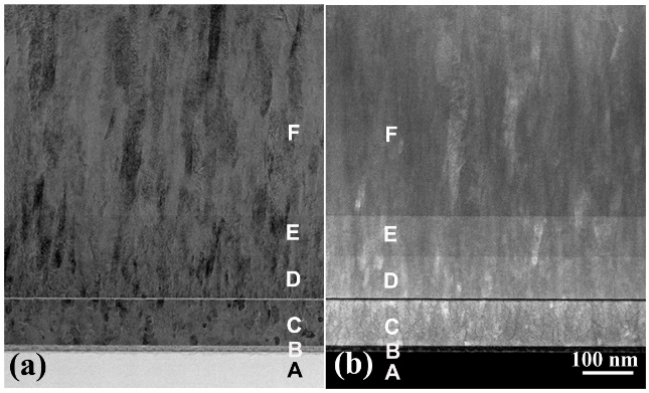

Figure 1: A cross-sectional BF-STEM image (a) and the corresponding HAADF-STEM image (b) of a Cr(Al)N/17vol. %Al_2O_3 layer (F) prepared on transition layers (B~E), deposited on the Si substrate (A) rotated at ω = 12 rpm.

deposition I. Layer B, which formed at the initial revolutions, was amorphous oxides (*a*-SiO_x, *a*-Al_2O_3) containing a small amount of Cr. Air leaked in at opening the valve of the Ar cylinder formed such oxides by sputtering in oxygen ion containing plasma [8, 12]. The presence of *bcc* Cr crystallites was confirmed in Layer C. The crystals probably contained some Al atoms so that we described it as Cr(Al) [8]. Figure 2 exhibits strong Al and weak O signals as well as strong Cr signals from Layer C. This implies the presence of *a*-Al_2O_3 particles in Layer C, in particular, in its initial stage. This is confirmed by a halo ring in its ED pattern that corresponds to the spacing of (113) α-Al_2O_3 and (400) γ-Al_2O_3, and also by amorphous-like contrast in HR-TEM images. The multilayered structure of Cr(Al) particle sub-layers and *a*-Al_2O_3 particle sub-layers, which was previously found in Layer C prepared at 1 rpm [8], was never observed in the present sample. The time when the revolving substrate was exposed to the plasma (in chamber P) and the time when the substrate was not in the plasma (in chamber Q) were both so short (~ 2.5 seconds) in each revolution that the *a*-Al_2O_3 particles could not form single cover sub-layers. The growth rate of Layer C is ~13.5

nm/min.

Layers D and E grew by deposition II and III, respectively. CrN crystallites with the NaCl-type structure formed in layers D and E, similar to the previous observation [8]. Figure 2 shows that Layers D and E included Cr, Al, and N atoms with a small number of O atoms. The formation of *a*-Al_2O_3 particles as well as the CrN crystallites was confirmed with the aid of HR-TEM. These *a*-Al_2O_3 particles were dispersed in the layers and any multi-layered structure, which was observed within the Layers D and E prepared at ω = 1 rpm [8], did not form in the present layers. From observed thickness of the layers, the growth rates of Layers D and E were estimated to be 3.4 nm/min (= 98 nm/29 min) and 2.5 nm/min (= 90 nm/36 min), respectively, which are much lower than that of Layer C. Therefore, the formation and growth of nitride were very slow as compared with that of metal Cr, which was deposited by non-reactive sputtering in deposition I. The growth rate of Layer D was higher than Layer E. This can be ascribed to a little formation of Cr particles because of poor N_2 during Layer D deposition. Therefore, the Ar (10 sccm) + N_2 (10 sccm) flow for deposition II can be regarded as a transitional atmosphere of non-reactive sputtering for metal [Cr(Al)] and reactive sputtering for nitride [CrN]. In Figure 2, the HAADF and Cr-K EDS intensities are higher in D

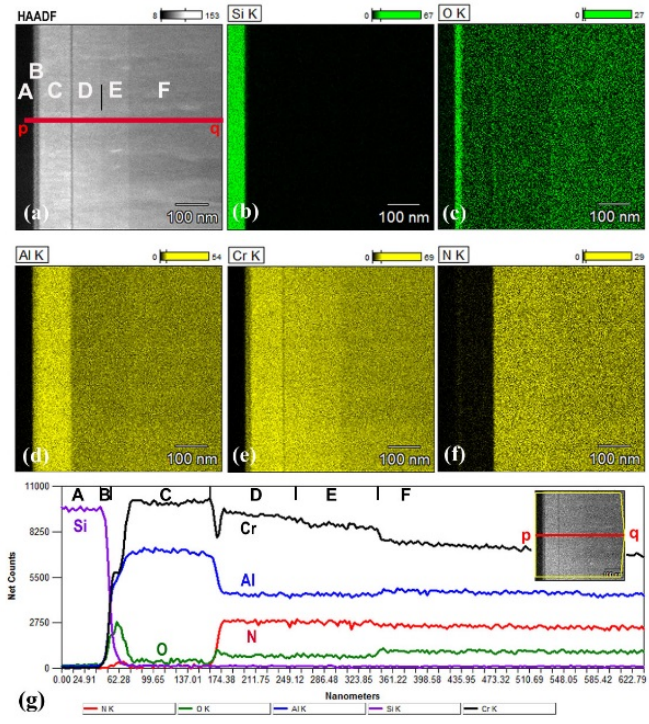

Figure 2: EDS analysis of the Cr(Al)N/17vol.%Al_2O_3 coating. (a) A HAADF STEM image of a cross section, normal to the substrate surface. (b-f) The corresponding EDS maps of Si-K, O-K, Al-K, Cr-K, and N-K signals, respectively. (g) EDS line profiles by integrating the map intensities across the interfaces. The measured line is indicated in (a) and an inset of (g).

than E while the N-K EDS intensity is almost the same. This supports the presence of Cr crystal in D (by non-reactive sputtering) and the complete formation of CrN crystal in E by increase of N_2 flow (by reactive sputtering on the target). The composite films usually aim at surface coating of a metal such as steel. These transition buffer layers, where the composition gradually changes from metal (Cr) to nitride (CrN), are appropriate to the adhesion between the metal substrate and the composite nitride coating.

Layer F is the main Cr(Al)N/Al_2O_3 layer that formed in alternate half revolution during deposition IV from the CrAl target and the Al_2O_3 target. Layer F can be identified by less bright HAADF contrast, strong Al-K and O-K intensities, and weak Cr intensity compared with layer E (Fig. 2). The

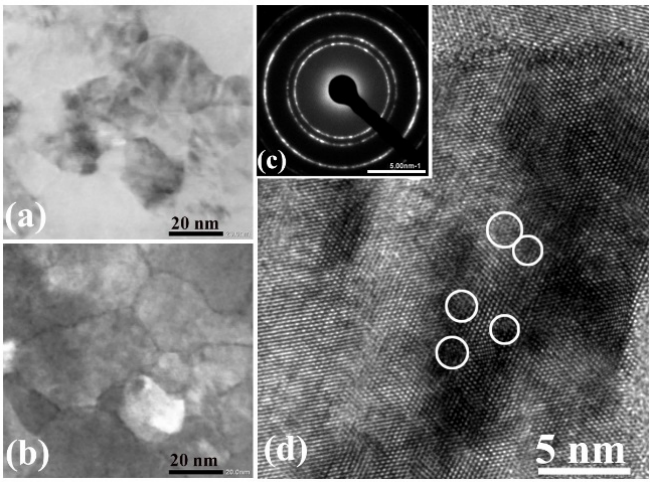

Figure 3: A BF-STEM image of a cross section, parallel to the substrate surface, of layer F. (a) and the corresponding HAADF-STEM image (b). An ED pattern (c) and an HR-TEM image (d) of a small area in (a).

differences are ascribed to the additional sputtering-deposition of Al_2O_3. The amount of revolutions was 9720 (= 12 rpm x 810 min). Figure 3 shows images of a cross section, parallel to the substrate surface, of Layer F. The STEM image contrast in Figure 1 indicates that Layer F grew in columnar structure extending, through Layers C, D, and E, normal to the substrate. These columns can be observed in the plane view images in Figures 3 (a) and (b). Grains with sizes of several ten nanometers correspond to the section of the columns. Any multilayered structure was not formed in the present F layer (as see in Fig. 2), unlike the Cr(Al)N/SiO_x nanocomposite layer, prepared at ω = 1 rpm, with a multilayered structure composed of crystallite Cr(Al)N sub-layers (~1.6 nm thick) and *a*-SiO_x sub-layers (~1 nm thick) [8]. The ED pattern in Figure 3(c) reveals the presence of CrN crystal with NaCl-type structure. The crystals probably contain some Al atoms so that we described it as Cr(Al)N [8]. The HR-TEM image in Figure 3(d) shows Cr(Al)N crystallites with lattice fringes and *a*-Al_2O_3 particles some of which are indicated by circles. These fine *a*-Al_2O_3 particles were homogeneously dispersive in the Cr(Al)N crystals.

The H_{IT} (and E^*) of the Cr(Al)N/17vol.%Al_2O_3 coating increased with increasing ω from 37 GPa (312 GPa) at ω = 2 rpm to 43 GPa (348 GPa) at ω = 12 rpm. With increasing oxide fraction, H_{IT} (and E^*) of the Cr(Al)N/Al_2O_3 coating prepared at ω = 12 rpm increased from 42.5 GPa (344 GPa) with Cr(Al)N to the maximum value with the Cr(Al)N/17vol.%Al_2O_3 coating and then decreased until H_{IT} = ~10 GPa with *a*-Al_2O_3. This shows that the hardness of nitride coating is improved by fabricating the nanocomposite layer. The Cr(Al)N/17vol.% Al_2O_3 film prepared at ω = 12 rpm was a super hard coating with H_{IT} = ~43 GPa, similar to Cr(Al)N/17 vol.% SiO_x film prepared at ω = 12 rpm (H_{IT} = 45 GPa) [9]. This can be ascribed to the fine *a*-Al_2O_3 particles, which can work as obstacles against the lattice deformation of Cr(Al)N. The increasing amount of amorphous oxide (>17 vol. %) reduces the supremacy of hard nitride and consequently softens the coating.

We demonstrated that the DPCS system allows us to fabricate super hard nanocomposite coating with a hardness of as high as ~45 GPa. DPCS has potential to fabricate harder coating by controlling preparation condition and searching target materials.

ACKNOWLEDGEMENTS

We are grateful to Mr. Hiroshi Takabatake and Mr. Takamasa Satoh, University of Toyama, for the sample preparation using DPCS and FIB. The author (M.N.) acknowledges Japan Society for the Promotion of Science (JSPS) and Osawa Scientific Studies Grants Foundation for the partial support from KAKENHI Grant Number 21360359 and OSG Study Grant in 2011, respectively.

REFERENCES

[1] J. Musil, Surf. Coat. Technol. **207**, 50 (2012).
[2] P. H. Mayrhofer, C. Mitterer, L. Hultman, H. Clements and H. Prog. Mater. Sci. **51**, 1032 (2006).
[3] S. Veprek and M.G.J. Veprek-Heijman, "*Nanostructured Coatings*", A. A.Cabaleiro and J. T. M. De Hosson, Eds., Springer, New York, 347-406, (2006).
[4] J. Lin, J. J. Moore, W.C. Moerbe, M. Pinkas, B. Mishra, G.L. Doll and W. D. Sproul, Int. J. Refract. Met. Hard Mater. **28**, 2 (2010).
[5] M. Stüber, U. Albers, H. Leiste, K. Seemann, C. Ziebert and S. Ulrich, Surf. Coat. Technol. **203**, 661 (2008).
[6] M. Kong, W. Zhao, Y. Wu, B. Huang and G. Li, J. Coat. Technol. Res. **9**, 177 (2012).
[7] M. Nose, T. Kurimoto, A. Saiki, M. Matsuda and K. Terayama, J. Vac. Sci. Technol. A, **30**, 011502, (2012).
[8] M. Kawasaki, H. Takabatake, I. Onishi, M. Nose and M. Shiojiri, ACS Appl. Mater. Interfaces. **5**, 3833 (2013).
[9] M. Kawasaki, M. Nose, I. Onishi and M. Shiojiri, Appl. Phys. Lett. **103**, 201913 (2013).
[10] S. Pennycook and P.D. Nellist, *Impact of Electron and Scanning Probe Microscopy on Materials Research*, D.G. Rickerby, G. Valdrè and U. Valdrè, Eds., Kluwer Academic Publishers: Dordrecht, 161−207, (1999).
[11] M. Shiojiri and H. Saijo, J. Microsc. **223**, 172 (2006).
[12] Y.Y. Chen, J.R. Yang, S.L. Cheng and M. Shiojiri. Thin Solid Films **545**, 183 (2013).